Quantum Information and Computation, Vol. 1, No. 2 (2001) 57–80

QUANTUM INFORMATION EXPERIMENTS WITH TRAPPED IONS: STATUS AND PROSPECTS

C. A. Sackett
Physics Department, University of Virginia
Charlottesville, VA 22911

Received (July 15, 2001)
Revised (July 28, 2001)

The current state of quantum information experiments using trapped ions is summarized. A brief review of the physics of ion traps is provided, along with an explanation of methods used to realize quantum logic operations. Some recent applications of these operations are discussed, along with prospects for further development.

1. Introduction

With recent developments in the general field of quantum information, it has become clear that quantum systems have the potential to yield significant advances in information technology [1–4]. Because of this potential, considerable experimental effort is underway to develop physical systems which are suitable for quantum information applications, in forms ranging from gas to liquid to solid state [3]. In the presence of so much activity, it becomes difficult to keep an overall perspective of these different approaches and what they have accomplished. It is the purpose of this review to help address this issue, by describing recent progress in techniques using trapped ions.

In the trapped-ion approach, individual charged atoms serve as quantum bits, and the interaction between qubits that is required for entanglement is provided by the Coulomb force. The ions are confined in an externally applied potential which is simple and well-characterized, and they are manipulated using laser beams, again in a very well-understood way. As a result, an extremely high degree of coherence and control is possible, while decoherence effects from the environment are relatively low. Furthermore, because the ions are trapped and prepared in definite states, quantum logic operations can be performed in a deterministic way, meaning that an operation has a reasonably high probability of success for each attempt. This is in contrast with some other approaches, in which the probability of success is low and signal is recovered either by averaging over many attempts [5] or by using coincidence techniques to identify those attempts which were successful [6, 7]. Many practical applications will require deterministic operations [8] of the type demonstrated in ion traps [9].

Other advantages of ion traps for quantum logic include nearly perfect state detection.

Detection accuracies of about 99% have been obtained, and even lower error probabilities should be possible. This can be compared with photon detection, in which efficiencies of about 10% are typically observed [6]. and field ionization of neutral atoms, which can achieve about 40% [7]. High efficiency is important for Bell inequality tests, and will also be necessary for reading out the state of a large quantum computer.

Due to these advantages, several groups worldwide are pursuing quantum information experiments in ion traps. Publicized efforts are underway at Aarhus aarhus, Ann Arbor[11], Hamburg [12], IBM-Almaden [13], Innsbruck [14], KARC [15], Los Alamos [16], MPQ-Garching [17], NIST-Boulder [18], and Oxford [19].

The paper consists of five sections. After this introduction, Section 2 reviews the basic physics of ion traps, and Section 3 discusses means by which quantum logic operations can be achieved. Section 4 then summarizes some recent applications and Section 5 outlines future directions for effort and offers concluding remarks. In the interests of space, some general background knowledge of quantum information science is assumed throughout.

2. Ion Trap Basics

In the trapped-ion approach, quantum information is stored in the internal states of the ions, while the external (motional) degrees of freedom are used for entanglement. It is necessary then for both parts of the quantum state to be highly controlled. In this section, requirements on the ion internal structure are first discussed, and then means of controlling the motion are addressed.

2.1. *Internal States*

Typically, ion species chosen for use in quantum logic experiments have only one valence electron, so that the internal states are basically similar to those of a neutral hydrogen or alkali metal atom. A large number of states are thus available, and it is necessary to select two which will serve as the qubit basis. One possibility is to use two sublevels of the electronic ground state, in which case quantum information is stored in the combined electronic and nuclear spins. Alternatively, one of the states can be a metastable excited state, so that information is stored in the electronic motion. This choice is a fundamental one, with each alternative having advantages and disadvantages.

If the qubit levels are both in the electronic ground state, then they are in principle extremely stable, with typical spontaneous emission rate on the order of 10^{-6} yr^{-1}. More likely causes of decoherence are fluctuating magnetic fields, which couple to the atomic spin. Nonetheless, coherence times of several hundred seconds have been achieved [20–22]. The effect of decoherence is quantified by the fidelity, F, defined to be $\langle\psi|\,\rho\,|\psi\rangle$ where ψ is the desired state and ρ is the actual density matrix. The fidelity is essentially given by the probability for a logic operation to succeed. For environmental decoherence, $1-F$ is given approximately by the ratio of operation time to decoherence time. The ground state sublevels are typically separated by microwave or radio frequencies, so coherent transitions could be driven between them by direct application of microwave or rf fields. The transition rate Ω is fundamentally limited to be small compared to the transition

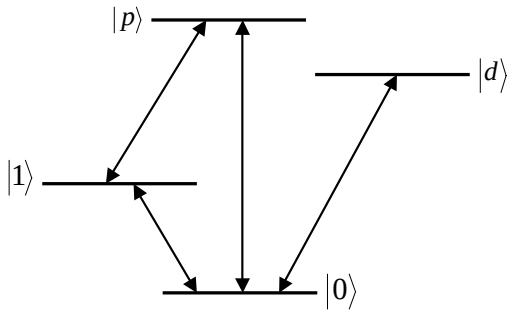

Fig. 1. Schematic of internal state structure required for quantum logic. States $|0\rangle$ and $|1\rangle$ are metastable states which store the quantum information. State $|p\rangle$ is used for optical pumping, in order to prepare the ion in a known state. State $|d\rangle$ is used for detection via state-selective fluorescence. Arrows show the required transition pathways.

frequency ω_0, but in practice power requirements limit the rate to roughly 10^6 s^{-1}. This gives a potential fidelity on the order of $1 - 10^{-8}$, where it is thought that fault-tolerant quantum computation requires $1 - F \sim 10^{-5}$ [23].

The two sublevels can also be coupled using a stimulated Raman transition, in which two laser beams are applied with frequencies that differ by an amount equal to the sublevel splitting. The lasers themselves are tuned near an excited state, so that a resonantly enhanced two-photon transition can occur. In this case, somewhat higher transition rates can be achieved, but spontaneous scattering is also allowed and this is a source of decoherence. This effect limits current experiments to $1 - F \approx 10^{-3} - 10^{-2}$, and it may be difficult to improve these values much beyond $\sim 10^{-4}$. This is worse than the direct microwave excitation approach, but the Raman technique allows coupling between the qubit states and the motion of the ions. This coupling is required for entanglement in the approaches that will be described below, but other alternatives have recently been suggested [24].

In contrast, if one of the qubit states is an electronic excited state, then the transition frequency will typically be optical, and the internal and motional states can be coupled directly by a laser. The lifetime of the excited state will necessarily be limited by spontaneous emission, but states exist which have lifetimes of seconds or more [25]. Coherent transition rates $\Omega \approx 10^6$ s^{-1} have been observed for single ion transitions [26], and significantly faster rates should be possible. Although entangling operations are likely to be slower [27], prospects for achieving high fidelity gates seem good. However, in order to take advantage of long coherence times, the driving laser must be very stable. Laser frequency stabilities below 1 Hz have been achieved in other experiments [28], but doing so is technically difficult. This requirement is the main disadvantage of the optical approach compared to the use of ground state sublevels, as the microwave frequency modulation required for Raman coupling is considerably simpler.

Besides the two qubit levels, in general at least two other internal states are required. The states are illustrated schematically in Fig. 1, and two experimental implementations

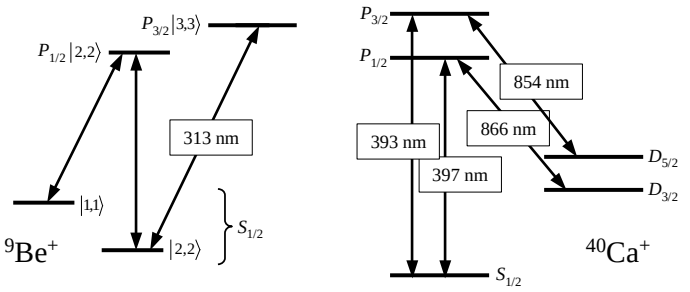

Fig. 2. Implementations of internal state structure in $^9Be^+$ and $^{40}Ca^+$. Here only strongly allowed transitions are shown. (a) In $^9Be^+$, the logic states $|0\rangle$ and $|1\rangle$ are, for example, the ground hyperfine levels $|2,-2\rangle$ and $|1,-1\rangle$ respectively, where in $|F,m_F\rangle$, F is the total angular momentum quantum number and m_F is the projection of the angular momentum along a chosen quantization axis. The two states are split by a frequency of approximately 1.25 GHz. States $|p\rangle$ and $|d\rangle$ are in the excited P_J manifold, where J is the total electronic angular momentum. The $P_{1/2}$ and $P_{3/2}$ states are separated by the fine structure splitting of $\sim$200 GHz. The radiative lifetime of the P states is 8 ns. Owing to angular momentum conservation, the $P_{3/2}\,|3,3\rangle$ hyperfine state can decay only to the $S_{1/2}\,|2,2\rangle$ state, making it suitable for detection. (b) In $^{40}Ca^+$, there is no nuclear spin and thus no hyperfine structure. In each of the states shown, the sublevel with maximum spin projection $m_J = J$ is used. Here the logic states are $|0\rangle \equiv S_{1/2}$ and $|1\rangle \equiv D_{5/2}$, which are separated with a transition wavelength of 729 nm. The lifetime of the $D_{5/2}$ state is approximately 1 s [30]. For detection, the ion is illuminated with laser light at 397 nm and 866 nm. No fluorescence is observed if the ion is in the $D_{5/2}$ state, while photons are scattered if it is in the $S_{1/2}$ state. The $P_{3/2}$ state is used for repumping.

are shown in Fig. 2. Here $|0\rangle$ and $|1\rangle$ denote the qubit levels. State $|p\rangle$ is an unstable excited state which is radiatively connected to both qubit states, and it is used to initially prepare the ion in a known state. This is done by optical pumping [29], where only one of the transitions, say $|1\rangle \leftrightarrow |p\rangle$, is driven until all of the population has decayed by spontaneous emission into $|0\rangle$. State preparation fidelities of 0.99 or greater have been achieved by this method.

The second excited state, $|d\rangle$, is radiatively connected only to one of the qubit states, shown here as $|0\rangle$. This is used to detect the state of the ions when the experiment is complete. If an ion is in $|0\rangle$ when the $|0\rangle \leftrightarrow |d\rangle$ transition is driven, it will fluoresce brightly as the ion cycles between the two states. In contrast, an ion in $|1\rangle$ will not participate in the transition, and will thus remain dark [31–33]. The number of photons emitted by the bright state can be 10^5 or more, which is large enough that the qubit states can be efficiently distinguished even if the efficiency for detecting a single photon is low. Figure 3 shows the results obtained using this detection procedure with two $^9Be^+$ ions. Here the states of the two ions a and b were detected jointly, so that $|0\rangle_a\,|1\rangle_b$ and $|1\rangle_a\,|0\rangle_b$ could not be distinguished. For a single ion, detection efficiencies of $\sim$0.99 have been demonstrated [34]. As can be seen from the figure, joint detection of multiple ions becomes more difficult unless an imaging technique is used to resolve each ion independently [35].

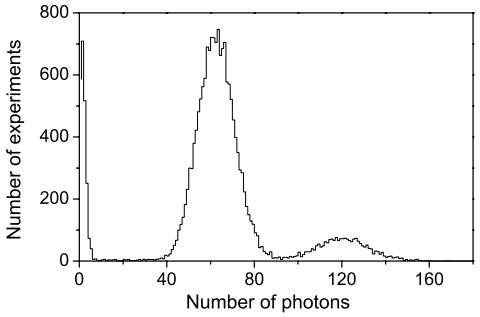

Fig. 3. Histogram showing detection of two $^9Be^+$ ions. When the ions repeated prepared in state ψ are illuminated with the detection laser beam, ion i fluoresces brightly with probability $|\langle\psi\,|0\rangle_i\,|^2$. (In order to suppress fluorescence from the $|1\rangle$ state, the population of the $|1\rangle \equiv |1,-1\rangle$ state is transferred to the $|1,1\rangle$ hyperfine state before detection.) On average, approximately 60 photons are detected from each fluorescing ion, but shot noise causes this number to fluctuate according to Poissonian statistics. The histogram shows the results obtained when the ions are identically prepared and detected 2×10^4 times in succession. The three peaks correspond to the possibilities that 0, 1 or 2 ions were found in state $|0\rangle$, and from the areas under the peaks, the respective probabilities can be determined.

A variety of ion species exist which meet these requirements. In addition to Be (Ref. [36]) and Ca (Ref. [37–39]), the remaining alkaline earths Mg (Ref. [40]), Sr and Ba (Ref. [41]) are being explored for use in quantum information experiments. The selection of an ion is based both on how well it supports the level structure of Fig. 1, and on the availability of lasers at the required wavelengths.

2.2. *Motion*

Given an ion with suitable internal states, a trap is required to hold it. It is impossible to trap a charged particle in free space using static electric fields [42], so ion trap designs either use time-dependent electric fields in radio-frequency (Paul) traps, or use a combination of electric and magnetic fields in Penning traps [43, 44]. It is difficult to stably localize small numbers of ions in a Penning trap, so quantum information experiments to date have used rf traps. In these traps, an electric field E oscillates rapidly compared to the frequencies of the ions' overall motion, and the time-averaged effect on the ions can be described by a pondermotive pseudopotential

$$U_p(\mathbf{r}) = \frac{q^2}{2M\Omega_T^2}\langle E(\mathbf{r})^2\rangle. \tag{1}$$

Here q is the ion's charge, M is its mass, Ω_T is the oscillation frequency of the field, and $\langle E^2\rangle$ denotes the time average. For a quadrupole field $E(\mathbf{r}) \sim r$, so the confining force is harmonic. In addition to the pondermotive trapping, the field also imposes a small

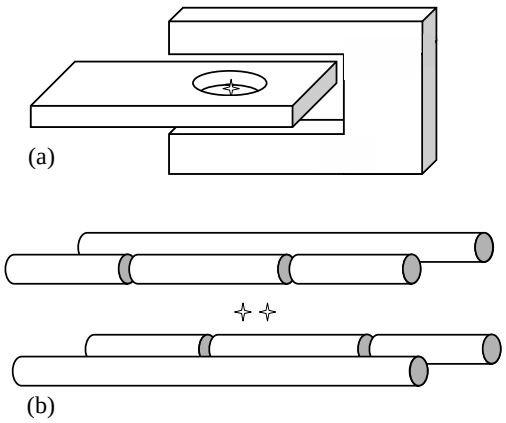

Fig. 4. Radio-frequency trap geometries. In both sketches, stars show the locations of trapped ions. (a) A spherical quadrupole trap can be formed using two electrodes, one with a hole and the other with a slot. An rf potential is applied between the two, resulting in a quadrupole field with a node at the center of the hole. (b) A linear trap consists of four parallel rods. An rf voltage is applied to the continuous rods shown, while the segmented rods are held at a dc potential. This gives an oscillating field which is zero along a line between the rods. To provide axial confinement, a positive voltage is applied to the outer segments of the dc rods, while the inner segments are held at ground or a negative potential.

amplitude oscillation at the rf frequency Ω onto the ions' motion. Termed micromotion, this oscillation has a spatially dependent amplitude $qE(\mathbf{r})/M\Omega_T^2$.

Two different field geometries are possible. In the first, the quadrupole field is a spherical quadrupole,

$$\mathbf{E}_{\text{sphere}}(\mathbf{r}) \propto a_x\mathbf{x} + a_y\mathbf{y} - (a_x + a_y)\mathbf{z}, \tag{2}$$

where $\mathbf{r} = \mathbf{x} + \mathbf{y} + \mathbf{z}$, and the asymmetry a_x/a_y is determined by the geometry of the trapping electrodes. One way to realize a field of this type is shown in Fig. 4(a). The second geometry uses a linear quadrupole field,

$$\mathbf{E}_{\text{lin}}(\mathbf{r}) \propto a_x\mathbf{x} - a_y\mathbf{y}. \tag{3}$$

This provides pondermotive confinement in the radial directions only, so a static quadrupole field is used to obtain harmonic axial confinement. This geometry is illustrated in Fig. 4(b). In either case, typical harmonic oscillation frequencies range from 0.1 to 10 MHz, with rf frequencies roughly 10 times higher.

For a single ion, the spherical and linear geometries are basically equivalent, but this is not the case when multiple ions are trapped. As discussed below, the ions can be cooled nearly to the ground state of the potential [45]. The motions of the cold ions are strongly coupled by the Coulomb interaction, so the ground state is a crystalline arrangement occupying nonzero volume. In general then, most of the ions will experience a nonzero value of the pondermotive field and undergo micromotion. The micromotion has several

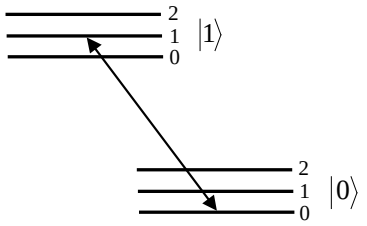

Fig. 5. The combined motional and internal states of a trapped ion. In the figure, internal states are labelled $|0\rangle$ and $|1\rangle$, and motional states are labelled as 0, 1, 2. Combined motional and spin transitions can be driven. The first blue sideband is illustrated.

deleterious effects when the ions are interacting with a laser, and it is therefore undesirable [36, 46–48]. It can be avoided in the linear geometry by making the axial confinement weak compared to the radial, so that the ions form a line along the z-axis where the rf field is zero. For increasing number of ions N, the axial confinement must be made weaker, with the ratio of axial to radial oscillation frequencies scaling as $N^{-0.9}$ for N large [49]. If the confinement is too weak it is difficult to keep the ions trapped and cold, and the slow motional frequencies limit the speed at which logic operations can be performed [27]. The number of ions that can be used is therefore limited.

Because the ions are strongly coupled, excitations from the ground state are described by normal modes of the ion crystal. There are $3N$ modes, and their frequencies and structures can be calculated by classical methods [50]. The simplest modes are the three center-of-mass (COM) modes, in which the ion crystal moves rigidly in the trap. The COM mode frequencies are the same as the oscillation frequencies of a single ion, independent of N.

Quantum mechanically, each mode i behaves to good approximation as a harmonic oscillator, with eigenstates $|n\rangle_i$, energies $n\hbar\omega_i$, and raising and lowering operators $a_i^\dagger$, a_i. Since all of the frequencies ω_i are typically large compared to the decoherence time, the motional states are well-defined, and must be included in the description of the quantum state. Fig. 5 illustrates the combined motional and internal states, for a particular motional mode of one ion. As shown, it is possible to drive transitions between motional states using the coupling field, such that $|0, n\rangle \leftrightarrow |1, n'\rangle$. The transition for $n = n'$ is termed the carrier, and occurs at frequency ω_0 independent of n. Transition with $n' = n \pm m$ are termed the mth blue (+) or red (-) sidebands, and have frequencies $\omega_0 \pm m\omega_i$. Thus, as long as the ω_i are not degenerate, a particular mode can be addressed by tuning the frequency of the coupling field. The states which are coupled will then undergo Rabi oscillation [26, 51] in the usual way [52].

For a single ion, the coupling strength of a motional transition can be characterized by the Lamb-Dicke parameter η. For ion mass M and mode frequency ω_i, the Lamb-Dicke

parameter is [a]

$$\eta_i = \left(\frac{\hbar}{2M\omega_i}\right)^{1/2} |\Delta\mathbf{k}\cdot\mathbf{u}_i|. \tag{4}$$

For a single photon transition, $\Delta\mathbf{k} = \mathbf{k}$, the wave vector of the driving field, while for a two-photon Raman transition, $\Delta\mathbf{k} = \mathbf{k}_1 - \mathbf{k}_2$. For a microwave transition, $\Delta\mathbf{k}$ is typically very small. Finally, $\mathbf{u}_i$ is a unit vector in the direction of oscillation of the ion. If the matrix element for the internal-state transition is $\hbar\Omega/2$, the Rabi frequency for the transition from n to $n' = n \pm m$ will be [53]

$$\Omega_{nn'} \equiv \Omega \langle n'| \exp i\eta_i(a_i + a_i^\dagger) |n\rangle = \Omega \left(\frac{n_>!}{n_<!}\right)^{1/2} e^{-\eta_i^2/2} \eta_i^m L_{n_<}^m(\eta_i^2) \tag{5}$$

where $n_>$ and $n_<$ are respectively the larger and smaller of n and n', and L_n^m is the generalized Laguerre polynomial. It is usually optimal for η to be small compared to 1, so that only the leading terms in η are important. It cannot be too small, however, since the sideband transition rates vanish for $\eta \to 0$. Values of 0.1 to 0.4 are typical. In the limit $n\eta_i^2 \ll 1$, (5) becomes

$$\Omega_{nn'} \approx \Omega \left(\frac{n_>!}{n_<!}\right)^{1/2} \frac{\eta_i^m}{m!} \tag{6}$$

for a sideband transition, and

$$\Omega_{nn} \approx \Omega \left(1 - \frac{1+n}{2}\eta_i^2\right) \tag{7}$$

for the carrier. Note that each motional mode i will affect the carrier Rabi frequency as in (7).

The precise forms of Eqs. (5)-(7) are less important than the fact that in all cases, $\Omega_{nn'}$ depends on n. This is the reason that it is necessary to cool the ions' motion: if the ions are in an unknown motional state, then the Rabi frequency is also unknown and it is impossible to apply a precise transformation to the spin wave function. The resulting uncertainty is effectively a form of decoherence. For small η, this effect is weaker for the carrier transition than from the sidebands, but is nonetheless significant if high fidelity is desired.

Thus for quantum information applications, the ions must be cooled to their ground state. This can be achieved by several mechanisms. A representative one is sideband laser cooling [54], which can be understood with reference to Fig. 1. If the 'detection' state $|d\rangle$ has a linewidth γ which is smaller than the motional frequencies ω_i, the the states $|D, n\rangle$ will be resolved. When η is small, spontaneous decay from $|d\rangle$ to $|0\rangle$ will tend to conserve n. So, by tuning a laser to the $|0, n\rangle \leftrightarrow |D, n-1\rangle$ transition, approximately one quantum will be removed from the motional mode in each excitation/decay cycle. This cooling proceeds until the mode's mean excitation $\langle n\rangle$ is approximately $(\gamma/2\omega_i)^2$, which is close to zero in the resolved sideband limit.

[a] For more than one ion, a similar analysis applies, but the Lamb-Dicke parameters η_i have a more complicated form [36, 50].

Effective sideband cooling has been observed [26, 45, 55], but typical implementations are more complicated, because usually state $|d\rangle$ does not have $\gamma \ll \omega_i$. One solution is to cool on the $|0\rangle \leftrightarrow |1\rangle$ transition, and to use the $|1\rangle \rightarrow |p\rangle$ transition to obtain the necessary spontaneous decay step [56]. Alternatively, another laser can be used to impart additional structure to the $|d\rangle$ state, generating an effectively narrower linewidth γ [57]. By such methods, single mode ground state populations of up to 99.9% have been obtained [57].

Unfortunately, the ions do not remain cold indefinitely. Being charged, the ions interact with fluctuating ambient electric fields, which leads to heating [58]. The COM modes couple directly to the ambient field, while other modes couple to its higher moments. For relatively distant field sources, the higher moments are greatly reduced, so only the COM modes are observed to heat [59]. The measured heating rates are generally too large to be explained by known ambient field sources, including thermal blackbody radiation. It is hypothesized that the anomalous effect is due to fluctuating surface charge distributions on the trap electrodes. A model based on this assumption predicts that the heating rate scales as [58]

$$\frac{d\langle n\rangle}{dt} \propto \frac{N}{M\omega d^4} S(\omega), \tag{8}$$

where N is the number of ions, M is the mass of a single ion, ω is the mode frequency, d is the distance to the electrode surface, and $S(\omega)$ is the noise power spectral density. Available data on heating rates roughly follow this scaling law, with $S \propto \omega^{-\beta}$ for β typically between 0 and 1. Typical heating rates are $d\langle n\rangle/dt \approx 2 \times 10^3$ s^{-1} for ^{9}Be$^+$ ions in a trap with $d \approx 300$ μm and $\omega \approx 2\pi \times 10$ MHz [58], and 5 s^{-1} for ^{40}Ca$^+$ ions in a trap with $d \approx 700$ μm and $\omega \approx 2\pi \times 4$ MHz [57]. These values agree with the above scaling to about an order of magnitude. Some techniques for combating or reducing the effects of this heating are described in Section 5.

3. Quantum Logic

As discussed above, there are several ways to implement an effective two-level system for quantum logic using a trapped ion. General quantum logic operations then require the ability to apply arbitrary unitary transformations to any single qubit, as well as an entangling operation between any pair of qubits. These requirements are discussed in turn.

3.1. *Single Qubit Operations*

Transformations of the state of a single ion are obtained by coherently driving the $|0\rangle \leftrightarrow |1\rangle$ carrier transition for a time t and with phase ϕ.[b] Working in the interaction picture, the effect of the transition can be described by a rotation operation $R(\Omega t, \phi)$, where

$$R(\theta, \phi) = \begin{bmatrix} \cos(\theta/2) & e^{i\phi}\sin(\theta/2) \\ -e^{-i\phi}\sin(\theta/2) & \cos(\theta/2) \end{bmatrix} \tag{9}$$

in the $\{|0\rangle, |1\rangle\}$ basis. Here Ω is the Rabi frequency. For $\theta = \pi$, rotation fidelities on

[b] For a direct transition, ϕ is the phase of the laser field, while for a Raman transition it is the phase of the beat note between the two beams at the position of the ion.

the order of 0.98 have been achieved, with imperfections due to laser noise, magnetic field fluctuations, spontaneous emission, and motional heating.

This rotation operation is sufficient to generate arbitrary single-qubit transformations. In a collection of several ions, however, it is necessary to apply (9) to each ion independently. The separation between the ions is approximately

$$s = \left(\frac{e^2}{4\pi\epsilon_0 M\omega^2} \right)^{1/3} \tag{10}$$

For traps with oscillation frequencies of a few MHz, s is typically a few μm, so that focusing a laser beam onto a single ion while avoiding its neighbors is nontrivial. The best results to date have been achieved using $^{40}Ca^+$ ions in a trap with axial frequency $\omega_z = 2\pi \times 700$ kHz, where 729 nm coupling light was applied to individual ions at a separation of 6.6 μm [60]. As noted, however, higher oscillation frequencies are generally advantageous.

One alternative solution makes use of the fact that the phase ϕ appearing in (9) is in general a function of the location of the ion $\mathbf{r}_i$,

$$\phi = \phi_0 + \Delta\mathbf{k} \cdot \mathbf{r}_i \tag{11}$$

where ϕ_0 is the phase of the drive field at the reference position $\mathbf{r}_i = 0$ and $\Delta\mathbf{k}$ is the same as in (4). By manipulating the positions of the ions, differential phase shifts can be obtained while allowing all the ions to be illuminated. For instance, if two ions are in the trap and are equally illuminated, a rotation by θ on one ion only is achieved in three steps. First, a laser pulse is used to rotate both ions by $\theta/2$. The trap electrode voltages are then adjusted so that one ion remains fixed, but the other is displaced by an amount $\mathbf{d}$ with $\Delta\mathbf{k} \cdot \mathbf{d} = \pi$. A second laser pulse identical to the first is then applied, which completes the rotation of the first ion, but reverses the rotation of the second ion. This technique has been demonstrated for two ions, with a fidelity of approximately 0.95 [61]. It can be generalized for more ions, but the pulse sequence complexity grows rapidly.

3.2. *Entanglement*

Entanglement of two particles requires some form of interaction to exist between them. In the case of ions, this interaction is provided by the Coulomb force, which causes the motion of different ions to be coupled. Several schemes have been proposed which take advantage of this coupling [9, 24, 36, 62, **?**, 63, 65–68]. The methods which have been successfully implemented are described here.

The original proposal to use trapped ions for quantum logic was by Cirac and Zoller (CZ) [62]. Their entanglement method requires a third stable atomic state $|2\rangle$ in addition to $|0\rangle$ and $|1\rangle$. Entanglement between two ions i and j is then achieved in the form of a phase gate, in which ion j acquires a phase of π if both ions i and j are in state $|1\rangle$. Assuming the ions can be individually addressed and the motion is initially in the ground state, the required pulse sequence is:

(i) The red sideband transition of ion i is driven with $\theta = \pi$ in Eq. (9). This transfers

the state of the ion to the motion:

$$(\alpha \left|0\right\rangle_i + \beta \left|1\right\rangle_i) \left|0\right\rangle_m \rightarrow \left|0\right\rangle_i (\alpha \left|0\right\rangle_m + \beta \left|1\right\rangle_m), \tag{12}$$

where the subscript i denotes the internal state of ion i and m denotes the motional state of the mode being used.

(ii) The $\left|1\right\rangle_j \left|1\right\rangle_m \leftrightarrow \left|2\right\rangle_j \left|0\right\rangle_m$ transition on ion j is driven with $\theta = 2\pi$. This introduces a phase shift if the ion is in state $\left|1\right\rangle$ and the motional state is $\left|1\right\rangle$:

$$\left|1\right\rangle_j \left|1\right\rangle_m \rightarrow - \left|1\right\rangle_j \left|1\right\rangle_m . \tag{13}$$

(iii) The motional state is then mapped back onto ion i by reversing step (i), by driving the red sideband of ion i using $\theta = \pi$ and $\phi = \pi$.

The resulting phase gate is sufficient for universal quantum logic. The basis of it was demonstrated in Ref. [69], where a single ion was used and the motional state itself served as the control qubit.

Several more recent proposals have some advantages over the original CZ scheme. First, the CZ method requires individual addressing of the ions, which is experimentally difficult as noted above. It also requires the additional state $\left|2\right\rangle$. A suitable state may not be conveniently accessible, especially if it is demanded that the $\left|1\right\rangle \leftrightarrow \left|2\right\rangle$ transition exhibit no first order Zeeman shift in a fluctuating magnetic field. Finally, since the scheme relies on sideband transitions, it is very sensitive to motional decoherence. Achieving a fidelity of F requires the mode being used to have a thermal excitation less than approximately $1 - F$ quanta.

The entanglement scheme which has been most successful is that of Mølmer and Sørensen (MS) [70–73]. In this approach, a motional mode is used to obtain an interaction between the ions, but the mode is driven off-resonance so that it is only virtually excited. As a consequence, sensitivity to motional excitation is reduced. The method also relies on illuminating all the ions that are being entangled. Individual addressing is still required if two ions out of a larger collection are to be coupled, but not if only two ions are present. The method also has no need of an auxiliary state.

The technique is illustrated in Fig. 6. Two fields are simultaneously applied to the ions. The first is at a frequency $\omega_B = \omega_0 + \omega_m \pm \delta$, and the second at $\omega_R = \omega_0 - \omega_m \mp \delta$. Here ω_0 is the carrier frequency, ω_m the mode frequency, and $\delta \ll \omega_m$ is a small detuning. As illustrated, the net effect is to couple $\left|00\right\rangle \leftrightarrow \left|11\right\rangle$ and $\left|10\right\rangle \leftrightarrow \left|01\right\rangle$. The effective Rabi frequency for the two-step transition is

$$\tilde{\Omega} = \frac{\eta^2 \Omega^2}{\delta} \tag{14}$$

for carrier Rabi frequency Ω and Lamb-Dicke parameter η, assuming $\eta \ll 1$. Then if the lasers are applied for a time t with $\tilde{\Omega} t = \pi/2$, the entangling operation

$$E = \frac{e^{i\pi/4}}{\sqrt{2}} \begin{bmatrix} 1 & 0 & 0 & i \\ 0 & 1 & i & 0 \\ 0 & i & 1 & 0 \\ i & 0 & 0 & 1 \end{bmatrix} \tag{15}$$

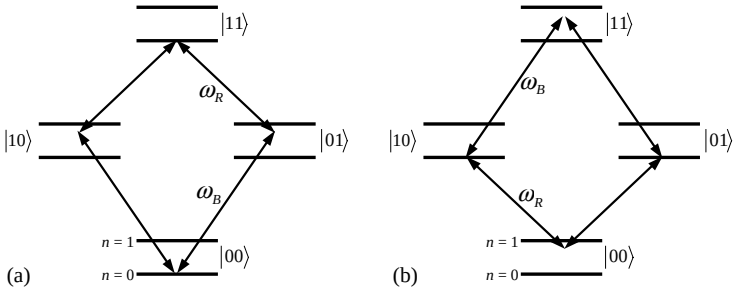

Fig. 6. The entangling operation of Mølmer and Sørensen. For two ions, the energy levels are as shown, where n labels the motional states of a particular mode. Entanglement is achieved by applying a bichromatic drive at frequencies ω_R and ω_B, which are slightly detuned from the red and blue sidebands, as shown. The effect is to couple (a) $|00\rangle \leftrightarrow |11\rangle$ and (b) $|10\rangle \leftrightarrow |10\rangle$, and by driving these transitions for an appropriate time, entangled states are created.

is realized. Here the state basis is $\{|00\rangle, |10\rangle, |01\rangle, |11\rangle\}$ and the phase convention is chosen such that the phase (11) at each ion is zero.

If δ is not too small, population of the intermediate states is negligible. The linewidth of the sideband transition is $\eta\Omega$, so avoiding motional excitation requires $\delta \gg \eta\Omega$. In order to increase $\tilde{\Omega}$, however, it is desirable that δ be as small as possible. This can be achieved by setting

$$\delta = 2\eta\Omega\sqrt{m} \tag{16}$$

for integer m, in which case the intermediate states are excited with mean quantum number $\langle n\rangle = (2m)^{-1}$, but the excitation vanishes at precisely the time (15) is realized [73]. For small m, however, the sensitivity of the operation to heating during the pulse is increased.

In addition to its other advantages, the MS technique can also be applied to multiple ions. For an even number of ions, application of the above fields results in the transformation

$$|0\ldots0\rangle \rightarrow |\psi_N\rangle \equiv \frac{1}{\sqrt{2}}\left(|0\ldots0\rangle + i^{N-1}|1\ldots1\rangle\right). \tag{17}$$

For an odd number, (17) can be achieved using one entangling pulse of the type described together with a uniform carrier rotation $R(\pi/2, 0)$ [71].

For the entangling operation to succeed, it is generally necessary for all the participating ions to have equal sideband Rabi frequencies $\eta\Omega$. For uniform illumination, this occurs for equal amplitudes of motional excitation. This is always the case if a COM mode is used for the intermediate state, but as noted above, the COM modes are subject to heating that limits the operation fidelity. In the cases of $N = 2$ and $N = 4$, there also exist symmetric "stretch" modes in which each ion's motional amplitude is the same. These modes were used in the experiments described below. In these cases, heating indirectly reduces the operation fidelity to [73]

$$F \approx 1 - \eta_{\mathrm{COM}}^4 \langle n\rangle(\langle n\rangle + 1)N(N-1) \tag{18}$$

where $\langle n \rangle$ is the average motional excitation of the COM mode. This is analogous to the effect on the carrier transition seen in (7), but the entangling operation is more sensitive for higher N.

The MS technique has been applied to $^9Be^+$ ions [74]. As seen in Fig. 2, $|0\rangle$ and $|1\rangle$ are ground hyperfine states. They are coupled by a Raman transition, and the two-step transition yielding (15) involves the exchange of four photons. The two Raman beams were aligned so that their difference wave vector was parallel to the trap axis, so that the lasers did not couple to the transverse motional modes.

The state $|\psi_N\rangle$ was prepared for $N = 2$ and 4. In both cases, the stretch mode frequency was 8.8 MHz, and the effective gate speed was $\tilde{\Omega} \approx 2\pi \times 25$ kHz. After the entanglement pulse, the detection method of Fig. 3 was used to determine the probabilities P_j that j ions were in state $|0\rangle$. For the two-ion case, $P_0 + P_2 \approx 0.95$, while for the four-ion case, $P_0 + P_4 \approx 0.70$. The coherence between the $|0 \ldots 0\rangle$ and $|1 \ldots 1\rangle$ states was measured by observing their interference after a uniform rotation $R(\pi/2, \phi)$. To illustrate this effect, in the ideal two-ion case, the rotation results in

$$|\psi_2\rangle \rightarrow \frac{1}{\sqrt{2}}\big(\,|00\rangle - i\,|11\rangle\,\big) \tag{19}$$

for $\phi = -\pi/4$, and

$$|\psi_2\rangle \rightarrow \frac{1}{\sqrt{2}}\big(\,|01\rangle + |10\rangle\,\big) \tag{20}$$

for $\phi = +\pi/4$. The average number of ions detected in state $|0\rangle$ is the same in either case, but whether the number is even or odd changes. In general, the parity

$$\Pi \equiv \sum_{j=0}^{N} (-1)^j P_j \tag{21}$$

oscillates as $\cos N\phi$, and the amplitude of the oscillation is $|2\rho_{0\ldots0,1\ldots1}|$, the far off-diagonal element of the density matrix ρ. Fig. 7 illustrates this oscillation.

From the population and coherence data, the fidelity of the entanglement operation $F = \langle\psi_N|\,\rho\,|\psi_N\rangle$ can be determined. For the two-ion case, the best observed fidelity is 0.92. It is believed that laser fluctuations, heating, and spontaneous emission all contribute to this error. The four-ion entanglement fidelity was 0.57. This case is more sensitive to heating, both because the COM mode frequency is lower and because of the $N(N-1)$ sensitivity noted above. The fidelity is, however, high enough to establish the existence of four-particle entanglement [74]. A four-photon entangled state has also been recently observed [75].

Prior to the above results, a pair of $^9Be^+$ ions were entangled using a different technique [9]. In that experiment, the two ions were confined in a spherical quadrupole trap, and the entanglement method made use of the micromotion oscillation described in Section 2.2. This approach was limited, however, by the difficulty of working with multiple ions in a spherical trap.

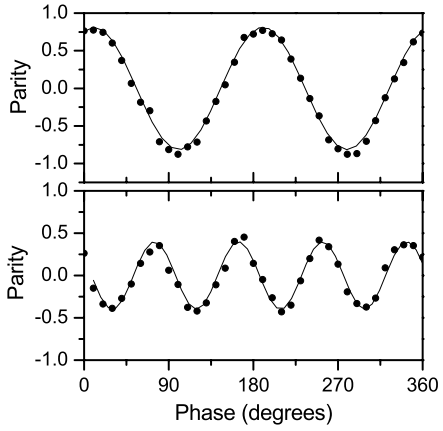

Fig. 7. Verification of entanglement. A state of the form $|\psi\rangle = (|0\ldots0\rangle + |1\ldots1\rangle)/\sqrt{2}$ is created, and then rotated into a transverse basis $(|0\rangle \pm e^{\pm i\phi}\,|1\rangle)/\sqrt{2}$. Upon detection, the parity (21) oscillates as $\cos N\phi$, where N is the number of ions. The amplitude of the oscillation gives the coherence of the original state.

Although entanglement of trapped ions has so far been achieved only using $^9Be^+$, it is not believed that other ion species are unsuitable. In particular, experiments on $^{40}Ca^+$ ions have demonstrated a high degree of coherence and control [26], and are expected to yield entanglement results in the near future.

4. Applications of Ion Entanglement

The four-particle entangled state described above is noteworthy, but still difficult to achieve reliably. Two-particle entanglement, however, is much more robust, and has been used as a basis for further studies. Three applications have been demonstrated: a violation of Bell's inequality [34], the encoding of a quantum state into a decoherence free subspace [61], and the use of entangled states to improve spectroscopic resolution [76].

4.1. *Bell's Inequality*

Bell's inequalities have long been used to contradict the notion of local realism. Loosely, this is the idea that objects have definite properties whether or not they are measured, and that these properties are not affected by events taking place sufficiently far away. Bell and others showed that all local realistic measurement predictions must obey certain inequalities, whereas quantum mechanics allows the inequalities to be violated [77–79]. Many experiments have since demonstrated violations of the inequalities [79, 80].

Experiments to date, however, have been subject to one or more significant loopholes,

allowing local realism to retain some viability. For instance, if the required measurements are not performed in a relativistically separate way, then it is possible for an unknown subluminal signal to affect the observed results. This locality loophole has been the subject of much experimental effort using entangled photon sources, starting with Ref. [81] and more recently in Refs. [82–84]. Whether these experiments have conclusively closed the locality loophole is still a matter of debate [85], but it seems clear that they have made local realistic theories increasingly implausible.

The second main loophole is due to the low detection efficiency of most experiments, which makes it possible that the totality of the events satisfies Bell's inequality even though the subensemble of detected events violates it [79]. Because ion states can be measured with near unit efficiency, the trapped-ion experiment closes this detection loophole for the first time. However, no experiment yet has simultaneously closed both loopholes, so again all that can be made is a plausibility argument.

The ion experiment tested the CHSH form of Bell's inequality [78]. Generically, the argument applies to a pair of spin-1/2 particles, prepared in an arbitrary state. A classical rotation of ϕ_1 is applied to particle 1, and ϕ_2 to particle 2. The spin projection of each particle along a fixed axis is then measured, and a correlation function q is assigned the value +1 if the two results agree, and -1 if not. This procedure is repeated many times for four combinations of rotation angles. Bell's inequality then states that the quantity

$$B(\alpha_1, \delta_1, \beta_2, \gamma_2) \equiv |\langle q(\delta_1, \gamma_2)\rangle - \langle q(\alpha_1, \gamma_2)\rangle| + |\langle q(\delta_1, \beta_2)\rangle + \langle q(\alpha_1, \beta_2)\rangle| \qquad (22)$$

must satisfy $B \leq 2$. Here α_1, δ_1, β_2, and γ_2 are rotation angles, and $\langle q(\phi_1, \phi_2)\rangle$ is the average correlation obtained using angles ϕ_1 and ϕ_2.

In the experiment, the entangled state $|\psi_2\rangle$ was generated by the MS technique. Rotations were applied using (9) on the carrier transition, for θ fixed at $\pi/2$. The phases ϕ_i played the role of the angles α, β, γ and δ, and were independently varied by adjusting the ion positions, as in (11). Detection was performed as in Fig. 3, with simple discriminator levels used to determine the number of ions in the bright $|0\rangle$ state for each experimental run. This number specified the value of q according to whether it was even or odd, since there is no need to distinguish which particle is in which state. The resulting state-detection accuracy was about 98%.

Quantum theory predicts Bell's inequality to be maximally violated for $\alpha_1 = \beta_2 = -\pi/8$ and $\delta_1 = \gamma_2 = 3\pi/8$, with $B = 2\sqrt{2}$. The experimentally obtained value was $B = 2.25 \pm 0.03$, which is consistent with the quantum prediction given experimental imperfections in state preparation, rotations, and detection.

4.2. *Decoherence Free Subspace*

Ultimate applications of quantum logic will likely rely on a variety of error correction and error avoidance methods to protect quantum data from weak interactions with a noisy environment [23]. One such method is to encode a qubit of information into a decoherence-free subspace (DFS) of several particles [86–89]. This protects the information from an environment which couples to each of the physical particles in the same way. For example,

trapped-ion quantum states suffer decoherence due to fluctuating ambient magnetic fields, which introduce an uncontrolled phase shift between $|0\rangle$ and $|1\rangle$. In this case, a DFS exists for two ions, spanned by the states $|01\rangle$ and $|10\rangle$, since any superposition of these states is unaffected by a uniform phase shift $|1\rangle \rightarrow e^{i\alpha}|1\rangle$.

In order for a DFS scheme to be useful, it must include a way to encode a qubit from the natural basis to the DFS. This can be accomplished for two ions using the Mølmer-Sørensen operation E. A two-qubit state of the form

$$|0\rangle (a|0\rangle + b|1\rangle) \tag{23}$$

was first prepared using the individual addressing technique of Section 3.1. Here the second ion holds the arbitrary qubit to be encoded, and the first serves as an ancilla qubit. Encoding was performed by applying E^{-1}, and then the operator $R_1(\pi/2, \pi/2) \otimes R_2(\pi/2, 0)$, where R_i is the carrier rotation operator (9) applied to ion i. The net effect is to transform the test state (23) to the encoded state

$$\frac{a}{\sqrt{2}}(|01\rangle + i|10\rangle) + \frac{b}{\sqrt{2}}(|01\rangle - i|10\rangle), \tag{24}$$

which is in the DFS. The E^{-1} operator was implemented by applying E three times, since $E^4 = 1$. Decoding is achieved by reversing these steps, applying $R_1(\pi/2, -\pi/2) \otimes R_2(\pi/2, \pi)$ and then E.

The encoding procedure was tested using Ramsey's method of separated fields [90]. First, in a control experiment, the second ion was rotated with $R_2(\pi/2, \beta)$, held for a fixed time, and then rotated again with a different phase, $R_2(\pi/2, \beta')$. The first ion remained in $|0\rangle$ throughout. The probability for the second ion to ultimately be in state $|0\rangle$ then oscillates as $\sin(\beta - \beta')$, and the contrast of this oscillation gives the coherence of the operations. Decoherence was introduced by illuminating both ions with a noisy laser beam that induced random ac-Stark shifts to the states. As seen in Fig. 8, the dephasing that resulted caused the contrast to rapidly decay as the duration of the noisy pulse was increased.

To see the effect of the DFS, the same experiment was performed, but the state of the second ion was encoded into the DFS before applying the noise, and decoded after. As the figure shows, in this case the noise had negligible effect. The unscaled contrast for the test state was 0.69 in the absence of noise, and for the encoding state it was 0.43. The encoding/decoding fidelity was therefore about 0.6, roughly consistent with the entangling fidelity of 0.9 since E was applied four times.

Resistance of the encoded state to naturally occurring decoherence was also observed, by performing the same two experiments but without the noisy pulse and with a variable time between the initial and final rotations. The unprotected state was found to decay with a time constant of 120 ± 20 μs, consistent with ambient magnetic field noise of several mG. The encoded state decay time was 450 ± 60 μs, which was presumably due to degradation of the decoding fidelity as the ions were heated.

4.3. *Improved Spectroscopic Resolution*

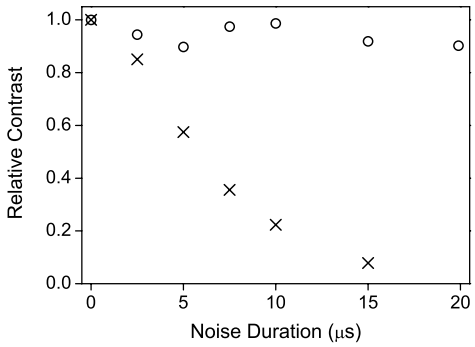

Fig. 8. Decay of the test state (crosses) and DFS encoded state (circles) under applied noise. Noise is applied for a fraction of the 25 μs delay between encoding and decoding, and the contrast of the Ramsey interference is measured. Contrasts are normalized to their values for no applied noise, to remove the effects of imperfect encoding operations.

Although not typically considered an aspect of quantum logic *per se*, one important motivating factor for studying entanglement is the possibility of increasing the sensitivity of quantum-limited measurements [91–98]. This is a very general effect: if a measurement O can be made on a single particle with accuracy $\Delta O = (\langle O^2\rangle - \langle O\rangle^2)^{1/2}$, then typically a measurement using N uncorrelated particles can reduce the uncertainty to $\Delta O/\sqrt{N}$. If the N particles are entangled, however, in some cases an uncertainty of $\Delta O/N$ can be achieved. This is the minimum possible value, termed the Heisenberg limit.

A demonstration of this effect was made using two $^9Be^+$ ions. A variety of methods for reducing measurement noise have been proposed, and several were investigated in Ref. [76]. We discuss here one used to demonstrate improved spectroscopic resolution of the $^9Be^+$hyperfine frequency [96].

The experiment is essentially a Ramsey experiment of the type described in the previous section. If the initial and final rotation pulses are driven at a fixed frequency ω which is detuned from the carrier frequency ω_0, then a phase $\Phi = (\omega - \omega_0)T$ accumulates during the variable time T between the two pulses. The final state oscillates with this phase, and by observing this oscillation, the detuning and thus ω_0 can be determined. For one measurement of a single ion, the phase can be determined with an accuracy of 1 rad, giving a frequency accuracy of $\delta\omega = 1/T$. For two unentangled ions, this is reduced by $\sqrt{2}$.

To improve this resolution, a state of the form $(|01\rangle + |10\rangle)/\sqrt{2}$ was produced by applying E to $|00\rangle$ followed by the uniform carrier rotation $R(\pi/2, \pi/4)$. The first Ramsey pulse $R(\pi/2, 0)$ then yields the state

$$\frac{1}{\sqrt{2}}(|00\rangle - |11\rangle) \tag{25}$$

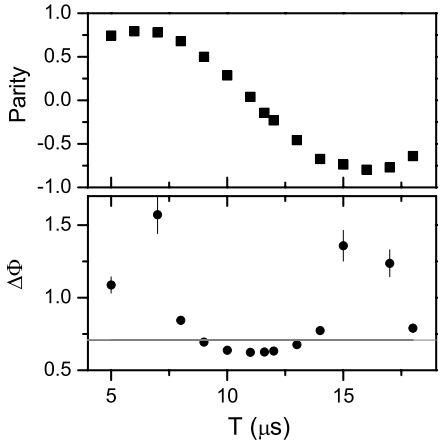

Fig. 9. Scheme for measurement of $^9Be^+$ hyperfine frequency using entanglement. A Ramsey experiment is performed using the initial state $(|01\rangle + |10\rangle)/\sqrt{2}$. (a) The parity Π is detected, and oscillates as $\cos 2\Phi$, where Φ is equal to $(\omega - \omega_0)T$ for drive frequency ω and resonant frequency ω_0. (b) The phase accuracy $\delta\Phi$, determined from the measured parity variance $\Delta\Pi$ and measured sensitivity $d\Pi/d\Phi$. When $\delta\Phi < 2^{-1/2}$ (the grey line shown), the frequency detuning $\omega - \omega_0$ is determined with an accuracy better than $1/(T\sqrt{2})$, which is the best accuracy that can possibly be achieved using unentangled ions. At the optimum time, $\delta\Phi = 0.62 \pm 0.01$.

which precesses to

$$\frac{1}{\sqrt{2}}\big(\,|00\rangle - e^{-2i\Phi}\,|11\rangle\,\big) \tag{26}$$

The final Ramsey pulse is again $R(\pi/2, 0)$, and the resulting state is

$$\frac{1}{\sqrt{2}}\big[-\cos\Phi\big(\,|01\rangle + |10\rangle\,\big) + i\sin\Phi\big(\,|00\rangle + |11\rangle\,\big)\big]. \tag{27}$$

As in Fig. 7, the parity Π oscillates, here as $-\cos 2\Phi$. Analogous to the single-ion signal, the phase of the parity oscillation can be determined with an accuracy of 1 rad, but since the parity oscillates twice as fast, the resulting frequency accuracy is $\delta\omega = 1/2T$.

The experimental result is shown in Fig. 9. The top graph shows the oscillation of the parity, while the bottom shows the phase accuracy

$$\delta\Phi = \frac{\Delta\Pi}{d\Pi/d\Phi} \tag{28}$$

As can be seen, a region exists where the observed accuracy is below the limit achievable without entanglement. This technique may ultimately be directly applicable to atomic clocks based on trapped ions.

5. Prospects

The above experiments indicate the ability to create and manipulate arbitrary two-particle quantum states. It is natural to ask, however, about the prospects for achieving similar results with larger numbers of ions. This is obviously a requirement for quantum computation, and would also be useful for spectroscopic improvements of the type described above. Although four-particle entanglement has been observed, further progress is impeded by the lack of easy individual addressing and by decoherence due to heating. Even if these problems are solved, it will likely prove difficult to work with many trapped ions, since the number of motional modes present grows quickly, and it becomes difficult to avoid mode cross-coupling [36, 99]. The ultimate limit of these effects is difficult to predict, but it seems unlikely that it will be possible to work with more than around ten ions in a trap.

5.1. *Heating*

To reach this goal, the anomalous heating described in Section 2.2 must be addressed. This is already a limitation in the two-ion $^9Be^+$ experiments. Results are encouraging, however, that this problem can be alleviated. Experiments using $^{40}Ca^+$ and ^{198}Hg have demonstrated much lower heating rates than typically observed in $^9Be^+$, suggesting that the larger traps of those experiments may be more suitable [45, 60]. Unfortunately, larger traps have lower motional frequencies, which reduces the potential gate speed and hampers cooling. However, low heating rates have also been observed in the $^9Be^+$ experiments [58], which indicates that conditions exist where the anomalous heating is reduced. With further study, it may be possible to identify these conditions; preliminary results suggest that shielding the electrodes from the ion source may be important.

A related approach is the exploration of new materials for use as trap electrodes. For instance, if the anomalous heating is caused by fluctuating patch potentials, the the use of single-crystal electrodes should be beneficial. In addition, current electrode structures are only able to withstand voltages of $\sim$1 kV before suffering catastrophic surface discharge. Better materials and processing may be able to significantly increase this value, thus allowing traps that are both strong and large.

Another promising possibility is the use of sympathetic cooling [40, 60, 100, 101]. Here one set of ions is used for quantum logic and another for cooling, so that the ion crystal can be cooled without affecting the internal states of the logic ions. If individual addressing is possible, this can be achieved by applying the cooling lasers only to the appropriate ions [60]. Alternatively, two different ion species can be trapped, and cooling lasers resonant with only one species used. To the extent that motional excitation is required for entanglement, the cooling cannot be applied during a gate, but it can be applied between operations, which may be sufficient. Also, several entanglement schemes have been proposed which do not require motional coherence [102], including the MS technique when used with a large intermediate state detuning. With such a method, cooling could be applied continuously [40]. A third alternative is to continuously cool the COM motion, while performing logic operations using another mode [101]. For instance, if a single cooling ion is positioned between two logic ions, the "stretch" mode of the logic ions is decoupled from the cooling ion. By keeping the COM mode cold, the decoherence of Eq. (18) would be avoided.

5.2. *Trap Arrays*

If the problem of heating can be solved, many experiments using small numbers of qubits will be enabled. For practical quantum computation, however, large numbers of qubits are required, and it is difficult to see how this can be achieved in a single trap. A promising approach, therefore, is to consider arrays of many traps, each of which contains only a few ions [103, 104]. Entanglement between ions in different traps could be achieved either by directly exchanging ions, or by coupling the ions to photons and exchanging photons between traps. Of these methods, direct ion exchange is simpler, but photon exchange may offer more promise.

A trap structure illustrating the idea of ion exchange is illustrated in Fig. 10. Here transverse confinement is provided by a pondermotive potential throughout the structure, but a series of dc electrodes allows the axial potential to be manipulated in a flexible way. For instance, a trap can be formed at position B by lowering the potential of electrode B and raising the potentials of A and C. If two ions are confined at B, they can be separated by first lowering C and D, and then raising C. One ion will then be left at position D, where it could be combined with a third ion at position F. The figure shows only a single linear array, but more complex structures are also possible, including T-like junctions.

After each logic operation, the internal and motional states are not coupled, so shuffling the ions between traps will not alter the stored qubits. It is unlikely, however, that the transfer can be performed adiabatically in the motional state, so it will be necessary to

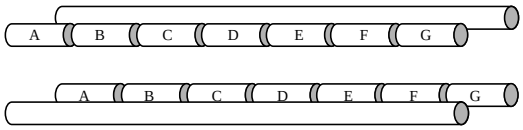

Fig. 10. An array of traps suitable for entangling multiple ions. Pondermotive radial confinement is provided as in 4(b), but several independent dc electrodes A-F allow ions to be shuffled back and forth along the structure.

recool the ions after a transfer. This can be achieved using sympathetic cooling, while still leaving the qubit state intact.

The speed of transfer between traps may be a liability in this scheme, and is yet to be experimentally investigated. A single ion can likely be transferred very quickly, but if two ions are to be separated, it may be necessary to change electrode voltages a rate comparable to the transverse confinement frequency. For large numbers of ions, many such steps may be required to bring two arbitrary ions together, which would have a significant impact on overall gate speed. It should be noted, however, that the practical limit on transverse confinement is not yet certain, and could conceivably reach frequencies of 100 MHz or greater. Also, it may be possible to minimize the number of transfer steps required by intelligent design of the array geometry and through tailoring of the algorithm to be implemented.

If photons, rather than ions, are exchanged, transfer speed is not a problem. In addition, the different trap regions could be maintained in different vacuum chambers, which would offer some convenience. Perhaps the chief advantage of coupling to photons, though, is that the photons could also be used for quantum communication applications [105]. Even a single ion coupled with a cavity would be a useful source of single photons [8, 106–108] while a larger network would be a promising platform for practical computation [109].

In principle, the required coupling can be achieved by placing an ion inside a high-finesse optical cavity and using quantum electrodynamic effects [110]. The effect has been demonstrated using neutral atomic beams [111, 112], and considerable effort is being made to trap both ions and neutral atoms in a cavity [113–117]. Substantial technical challenges remain: one difficulty for ion traps is the need to avoid electrical charging of the cavity mirrors, which must be both close to the ion and insulating. If the field from the mirrors is too strong, it can pull the ion out of the trap.

5.3. *Conclusions*

It is hoped that the discussion above has made a case that entanglement and quantum logic experiments with trapped ions have reached a stage of maturity where basic operations can be performed with some degree of reliability and repeatability. Quantum states can be prepared and detected with high accuracy, and a set of basic operations suitable for general quantum logic have been demonstrated with fidelities of around 0.95 per qubit.

The operations have been applied to a set of two ions, and a four-particle entangled state has been observed. These tools have been sufficient to demonstrate several applications, including a violation of Bell's inequality, a decoherence-free subspace encoding scheme, and improvements to spectroscopic resolution.

Experiments are currently limited by the anomalous heating effect, but approaches to solving this problem are available. When this problem is solved, prospects for scaling up to larger ion numbers will be good. While both the trap array and photon-coupling ideas pose difficult experimental challenges, the underlying atomic physics is well understood so there is good basis for optimism that these challenges can be overcome.

Acknowledgements

The work at N.I.S.T. described here was carried out by D. J. Wineland, C. Monroe, W. M. Itano, D. Kielpinski, V. Meyer, M. A. Rowe and Q. A. Turchette along with the author, and it was supported by the U.S. National Security agency and the Advanced Research and Development Agency under contract MOD-7171, by the U.S. Office of Naval Research, and by the US Army Research Office.

References

1. M. A. Nielsen and I. L. Chuang, *Quantum Computation and Quantum Information* (Cambridge Univeristy Press, Cambridge, 2000).
2. J. Preskill, *Lecture notes for Physics 229* (http://theory.caltech.edu/ preskill/ph229).
3. *Fortsch. Phys.*: Special issues on quatum computation, 4-6 **46** (1998) and 9-11 **48** (2000).
4. *J. Opt. B: Quantum Semiclass. Opt.*: Special issue on quatum computation and entanglement, **3**:1 (2001).
5. S. L. Braunstein *et al.*, *Phys. Rev. Lett.* (1999) **83**, 1054.
6. D. Bouwmeester *et al.*, *Phys. Rev. Lett.* (1999) **82**, 1345.
7. A. Rauschenbeutel *et al.*, *Science* (2000) **288**, 2024.
8. C. K. Law and H. J. Kimble, *J. Mod. Opt.* (1997) **44**, 2067.
9. Q. A. Turchette *et al.*, *Phys. Rev. Lett.* (1998) **81**, 3631.
10. Web address `http://www.ifa.au.dk/iontrapgroup`
11. Web address `http://monroelab2.physics.lsa.umich.edu/`
12. Web address `http://www.physnet.uni-hamburg.de/ilp/english/iontraps.html`
13. Web address `http://www.almaden.ibm.com/st/projects/quantum/ion`
14. Web address `http://heart-c704.uibk.ac.at`
15. Web address `http://www-karc.crl.go.jp/laser/index-E.html`
16. Web address `http://p23.lanl.gov/Quantum/quantum.html`
17. Web address `http://www.mpq.mpg.de/laserphysics.html`
18. Web address `http://www.boulder.nist.gov/timefreq/ion`
19. Web address `http://www.qubit.org/research/IonTrap`
20. J. J. Bollinger *et al.*, *IEEE Trans. on Instrum. and Measurement* (1991) **40**, 126.
21. P. T. H. Fisk, *Rep. Prog. Phys.* (1997) **60**, 1.
22. D. J. Berkeland *et al.*, *Phys. Rev. Lett.* (1998) **80**, 2089.
23. J. Preskill, *Phys. Today* (1999) **52**, 24.
24. F. Mintert and C. Wonderlich, quant-ph/0104041.
25. D. A. Church, *Phys. Reports* (1993) **228**, 253.
26. C. Roos *et al.*, *Phys. Rev. Lett.* (1999) **83**, 4713.

27. A. Steane *et al.*, *Phys. Rev. A* (2000) **62**, 042305.
28. B. C. Young, F. C. Cruz, W. M. Itano, and J. C. Bergquist, *Phys. Rev. Lett.* (1999) **82**, 3799.
29. W. Happer, *Rev. Mod. Phys.* (1970) **44**, 169.
30. P. A. Barton *et al.*, *Phys. Rev. A* (2000) **62**, 032503.
31. W. Nagourney, J. Sandberg, and H. G. Dehmelt, *Phys. Rev. Lett.* (1986) **56**, 2797.
32. T. Sauter, R. Blatt, W. Neuhauser, and P. E. Toschek, *Phys. Rev. Lett.* (1986) **57**, 1696.
33. J. C. Bergquist, R. G. Hulet, W. M. Itano, and D. J. Wineland, *Phys. Rev. Lett.* (1986) **57**, 1699.
34. M. A. Rowe *et al.*, *Nature* (2001) **409**, 791.
35. H. Nägerl *et al.*, *Phys. Rev. A* (1999) **60**, 145.
36. D. J. Wineland *et al.*, *J. Res. NIST* (1998) **103**, 259.
37. H. C. Nägerl *et al.*, *Phys. Rev. A* (2000) **61**, 023405.
38. R. Hughes *et al.*, *Fortsch. der Phys.* (1998) **46**, 329.
39. A. Stean, *Appl. Phys. B* (1997) **64**, 623.
40. G. Morigi and H. Walther, *Eur. Phys. J. D* (2001) **13**, 261.
41. R. G. DeVoe and R. G. Brewer, *Phys. Rev. Lett.* (1996) **76**, 2049.
42. S. Earnshaw, *Trans. Camb. Phil. Soc.* (1842) **7**, 97.
43. R. C. Thompson, *Adv. At. Mol. Opt. Phys.* (1993) **31**, 63.
44. P. K. Ghosh, *Ion Traps* (Clarendon, Oxford, 1995).
45. F. Diedrich, J. C. Bergquist, W. M. Itano, and D. J. Wineland, *Phys. Rev. Lett.* (1989) **62**, 403.
46. R. G. DeVoe, J. Hoffnagle, and R. G. Brewer, *Phys. Rev. A* (1989) **39**, 4362.
47. R. Blümel, C. Kappler, W. Quint, and H. Walther, *Phys. Rev. A* (1989) **40**, 808.
48. J. I. Cirac *et al.*, *Phys. Rev. A* (1994) **49**, 421.
49. D. G. Enzer *et al.*, *Phys. Rev. Lett.* (2000) **85**, 2466.
50. D. F. V. James, *Appl. Phys. B* (1998) **66**, 181.
51. D. M. Meekhof *et al.*, *Phys. Rev. Lett.* (1996) **76**, 1796.
52. C. Cohen-Tannoudji, B. Diu, and F. Laloë, *Quantum Mechanics* (John Wiley and Sons, New York, 1977), p. 405.
53. K. E. Kahill and R. J. Glauber, *Phys. Rev.* (1969) **177**, 1857.
54. D. J. Wineland and W. M. Itano, *Phys. Rev. A* (1979) **20**, 1521.
55. E. Peik *et al.*, *Phys. Rev. A* (1999) **60**, 439.
56. C. Monroe *et al.*, *Phys. Rev. Lett.* (1995) **75**, 4011.
57. C. F. Roos *et al.*, *Phys. Rev. Lett.* (2000) **85**, 5547.
58. Q. A. Turchette *et al.*, *Phys. Rev. A* (2000) **61**, 063418.
59. B. E. King *et al.*, *Phys. Rev. Lett.* (1998) **81**, 1525.
60. H. Rohde *et al.*, *J. Opt. B* (2001) **3**, S34.
61. D. Kielpinski *et al.*, *Science* (2001) **291**, 1013.
62. J. I. Cirac and P. Zoller, *Phys. Rev. Lett.* (1995) **74**, 4091.
63. J. F. Poyatos, J. I. Cirac, and P. Zoller, *Phys. Rev. Lett.* (1998) **81**, 1322.
64. G. J. Milburn, S. Schneider, and D. F. V. James, *Fortsch. der Phys.* (2000) **48**, 801.
65. J. I. Cirac and P. Zoller, *Nature* (2000) **404**, 499.
66. D. Jonathan, M. B. Plenio, and P. L. Knight, *Phys. Rev. A* (2000) **62**, 042307.
67. D. Jonathan and M. Plenio, quant-ph/0103140.
68. L.-M. Duan, J. I. Cirac, and P. Zoller, *Science* (2001) **292**, 1695.
69. C. Monroe *et al.*, *Phys. Rev. Lett.* (1995) **75**, 4714.
70. A. Sørensen and K. Mølmer, *Phys. Rev. Lett.* (1999) **82**, 1804.
71. K. Mølmer and A. Sørensen, *Phys. Rev. Lett.* (1999) **82**, 1835.
72. E. Solano, R. L. de Matos Filho, and N. Zagury, *Phys. Rev. A* (1999) **59**, R2539.
73. A. Sørensen and K. Mølmer, *Phys. Rev. A* (2000) **62**, 022311.

74. C. A. Sackett *et al.*, *Nature* (2000) **404**, 256.
75. J.-W. Pan *et al.*, *Phys. Rev. Lett.* (2001) **86**, 4435.
76. V. Meyer *et al.*, *Phys. Rev. Lett.* (2001) **86**, 5870.
77. J. S. Bell, *Physics* (1965) **1**, 195.
78. J. F. Clauser, M. A. Horne, A. Shimony, and R. A. Holt, *Phys. Rev. Lett.* (1969) **23**, 880.
79. J. F. Clauser and A. Shimony, *Rep. Prog. Phys.* (1978) **41**, 1883.
80. A. Aspect, *Nature* (1999) **398**, 189.
81. A. Aspect, P. Grangier, and G. Roger, *Phys. Rev. Lett.* (1982) **49**, 91.
82. W. Tittel, J. Brendel, H. Abinden, and N. Gisin, *Phys. Rev. Lett.* (1998) **81**, 3563.
83. G. Weihs *et al.*, *Phys. Rev. Lett.* (1998) **81**, 5039.
84. N. Gisin and H. Zbinden, *Phys. Lett. A* (1999) **264**, 103.
85. L. Vaidman, quant-ph/0102139.
86. D. A. Lidar, I. L. Chuang, and K. B. Whaley, *Phys. Rev. Lett.* (1998) **81**, 2594.
87. P. Zanardi and M. Rasetti, *Phys. Rev. Lett.* (1997) **79**, 3306.
88. L. M. Duan and G. C. Guo, *Phys. Rev. A* (1998) **57**, 737.
89. P. G. Kwiat, A. J. Berglund, J. B. Altepeter, and A. G. White, *Science* (2000) **290**, 498.
90. N. Ramsey, *Molecular Beams* (Clarendon Press, Oxford, 1956).
91. B. Yurke, *Phys. Rev. Lett.* (1986) **56**, 1515.
92. D. J. Wineland *et al.*, *Phys. Rev. A* (1992) **46**, R6797.
93. M. Kitagawa and M. Ueda, *Phys. Rev. A* (1993) **47**, 5138.
94. M. J. Holland and K. Burnett, *Phys. Rev. Lett.* (1993) **71**, 1355.
95. B. C. Saunders and G. J. Milburn, *Phys. Rev. Lett.* (1995) **75**, 2944.
96. J. J. Bollinger, W. M. Itano, D. J. Wineland, and D. J. Heinzen, *Phys. Rev. A* (1996) **54**, R4649.
97. P. Bouyer and M. A. Kasevich, *Phys. Rev. A* (1997) **56**, R1083.
98. T. Kim *et al.*, *Phys. Rev. A* (1998) **57**, 4004.
99. C. Monroe *et al.*, in *Atomic Physics 17*, edited by E. Arimondo, P. DeNatle, and M. Inguscio (AIP Conf. Proc. 551, Melville, NY, 2001), pp. 173–186.
100. D. Larson *et al.*, *Phys. Rev. A* (1986) **57**, 70.
101. D. Kielpinski *et al.*, *Phys. Rev. A* (2000) **61**, 032310.
102. D. F. V. James, *Fortsch. der Phys.* (2000) **48**, 823.
103. D. Wineland *et al.*, in *Atomic Physics 15*, edited by H. van Linden van den Heuvell, J. Walraven, and M. Reynolds (World Scientific, Singapore, 1997), pp. 31–46.
104. R. G. DeVoe, *Phys. Rev. A* (1998) **58**, 910.
105. D. Bouwmeester, A. Ekert, and A. Zeilinger, *The Physics of Quantum Information* (Springer, Berlin, 2000).
106. P. Domokos *et al.*, *Eur. Phys. J. D* (1998) **1**, 1.
107. A. Kuhn, M. Hennrich, T. Bondo, and G. Rempe, *Appl. Phys. B* (1999) **69**, 373.
108. S. Brattke, B. Varcoe, and H. Walter, *Phys. Rev. Lett.* (2001) **86**, 3534.
109. J. I. Cirac, P. Zoller, H. J. Kimble, and H. Mabuchi, *Phys. Rev. Lett.* (1997) **78**, 3221.
110. *Advances in Atomic, Molecular, and Optical Physics, Supplement 2*, edited by P. Berman (Academic Press, New York, 1993).
111. Q. A. Turchette *et al.*, *Phys. Rev. Lett.* (1995) **75**, 4710.
112. A. Rauschenbeutel *et al.*, *Phys. Rev. Lett.* (1999) **83**, 5166.
113. G. M. Meyer, H.-J. Briegel, and H. Walther, *Euro. Phys. Lett.* (1997) **37**, 317.
114. C. J. Hood *et al.*, *Science* (2000) **287**, 1447.
115. P. W. H. Pinkse, T. Fischer, P. Maunz, and G. Rempe, *Nature* (2000) **404**, 365.
116. D. Frese *et al.*, *Phys. Rev. Lett.* (2000) **85**, 3777.
117. F. Schmidt-Kaler *et al.*, in *The Physics of Quantum Information*, edited by D. Bouwmeester, A. Ekert, and A. Zeilinger (Springer, Berlin, 2000).